European Congress on Computational Methods
in Applied Sciences and Engineering (ECCOMAS 2012)
J. Eberhardsteiner et.al. (eds.)
Vienna, Austria, September 10-14, 2012

HIGH LIFT DEVICES DESIGN OF A SUPERSONIC TRANSPORT AIRCRAFT BASED ON 3D COMPUTATIONAL FLUID DYNAMICS

Michele Gaffuri[1], **and Joël Brezillon**[1]

[1]German Aerospace Center, Institute of Aerodynamics and Flow Technology
Lilienthalplatz 7, D-38108 Braunschweig
e-mail: {michele.gaffuri,joel.brezillon}@dlr.de

Keywords: CFD, optimization, Vortex dominated flow, High lift devices, Response surface method

Abstract. *This paper presents an aerodynamic optimization chain whose purpose is to find the optimal High Lift Devices' settings for a supersonic transport aircraft in take-off conditions. The automatic CFD process chain consists of several key elements: a CAD modeling software (Catia) that controls the aircraft's external shape; a CAD translator (Cadfix), used for converting the geometric data to a format usable by the mesher; an unstructured grid generator (Solar); a finite volume Reynolds-Averaged Navier-Stokes CFD code (DLR-TAU) for the evaluation of the aircraft's aerodynamic performances. This "CAD-in-the-loop" optimization chain has the advantage of delivering geometries in CAD format without loss of information due to conversion so that the final geometry can be directly used, for example to construct a model for wind tunnel testing. Furthermore, the unstructured mesh approach allows for the treatment of very complex geometries with relatively small effort, an important advantage compared to the more common (in optimization) structured multiblock approach. Two optimization strategies are used: a Response Surface Method (RSM) that relies on a Regression Kriging approach and the Simplex method. Both methods are found to be capable of solving this kind of optimization tasks and produce similar results.*

1 INTRODUCTION

After the retirement of the Concorde in 2003 there has been no push for a new "21st Century" supersonic airliner. The reason for this lack of interest is simple: with current technology a Concorde like plane would not meet the operating cost targets required by airline companies, especially during a financial crisis such as the one in which the world economy finds itself in. A different matter is the Supersonic Business Jet (SSBJ) market: here shorter flight times could justify an increase in direct operating costs in a market where time *is* money. Additionally a smaller plane could more easily meet current (and future) noise and emissions regulations. Lastly, a lighter airplane produces a smaller sonic boom and may allow, with advanced sonic boom shaping designs [1, 2], supersonic flight overland, a very important factor for the U.S. business aviation.

In order to ensure a reasonable range for a business jet the specific fuel consumption has to be minimized and therefore the wing planform is primarily designed with the supersonic cruise performance in mind. However, the low speed phase is of great importance since business jets are required to operate from general aviation airfield whose runways are sometimes as short as 1800 m. In addition, a high lift over drag ratio is required to ensure a high angle of climb thus reducing noise nuisances. It is therefore very important to design highly efficient high lift devices to improve the take-off and landing performances of such a plane.

The choice of which type of high lift devices to use for a supersonic wing is limited by the fact that the mechanisms have to fit inside the (very thin) wing, since flap track fairings would greatly increase the drag during supersonic cruise. For this reason it is very difficult to design slotted high lift devices, so that droop nose slats and plain flaps are usually chosen: the front and aft portions of the wing simply rotate to increase the airfoil chamber. Flaps are usually divided into sections to keep the actuator size small and to allow for differential deflection. This results in small gaps between adjacent sections to avoid collisions between them. These gaps make the estimation of the aerodynamic performances of the high lift system more difficult. The design problem is also complicated by the fact that the deployment of flaps induces a change in the pitching moment value, requiring a readjustment of the trim setting. The resulting change in trim drag can be important and has to be taken into account during the design.

Typical supersonic aircrafts have low aspect ratio, highly swept wings. This kind of wing generates much of its lift in low speed/high incidence conditions by creating vortical structures on the suction side. The air flow is thus very complex and can only be accurately predicted using high fidelity Computational Fluid Dynamics (CFD) methods [3, 4]. DLR put large effort into improving its numerical capabilities to accurately predict the aerodynamic performance of supersonic wings at low speed. At first structured meshes were used [5] and the process has been well validated against wind tunnel test (WTT) data. Structured meshes are however complex and time demanding to generate for complex geometries. In this respect the use of unstructured meshes is a clear step forward in versatility: similar accuracy can be obtained as with structured meshes, albeit with some overhead regarding the mesh size and the associated computational time [6].

Due to the complexity of the flow it is difficult to know beforehand which flap settings are going to have good aerodynamic performances. It is therefore necessary to perform a more or less systematic exploration of all possible solutions (the so called "design space"). This can be efficiently accomplished by using an automatic optimization chain. Since the exploration time would be prohibitive if done manually, it is proposed in this paper to use an optimization process chain consisting of an optimizer, a CAD (Computer-Aided Design) modeler, an unstructured

grid generator and a CFD solver. The advantages of having a CAD modeler in the chain ("CAD in the loop" approach) are that complex movements can be accomplished more easily on the parametric geometry than on the discretized grid, and that the optimal geometry is directly available in CAD format, and can be later used for building a wind tunnel model, for example. When coupled with an unstructured mesh process this approach allows for the analysis of very complex geometries. A method for the trim process is also proposed. It relies on an assessment of the pitching moment derivative with respect to the horizontal tail plane (HTP) deflection to estimate the required HTP position and a mesh deformation process for rotating the HTP.

In the next section the test case chosen to assess the process chain performance is outlined, followed by a detailed description of the optimization chain itself and the tools used, while in the last two sections the optimization results are presented and analyzed in detail.

2 TEST CASE

The optimization's goal is to define optimal high lift devices' settings for the take-off condition of a supersonic transport aircraft. The configuration considered is JAXA's Quiet small Supersonic Transport (QsST, Figure 1), a small (50 passengers) airliner capable of flying at Mach 1.6 for 3500 nautical miles. The criterion chosen for evaluating the take-off performance is the lift over drag ratio (L/D) with 3 constraints: the lift coefficient CL has to exceed a given value, the aircraft has to be in a trimmed state and the angle of attack α cannot exceed a certain value (Table 1).

Figure 1: JAXA QsST configuration.

Constraint	Type	Value
Cm(CG)	=	0
CL	>=	0.5
AoA	<=	12°

Table 1: Constraints of the optimization problem.

There are 5 design parameters: the deflection angles of the 4 hinged-nose leading edge flaps and of the trailing edge plain flap (table 2); deflection angles are defined perpendicular to the hinge line (Figures 2, 3). Additionally the all-moving horizontal tail plane (HTP) can be adjusted to ensure trim, while the constraint on the lift coefficient is ensured via changes of α.

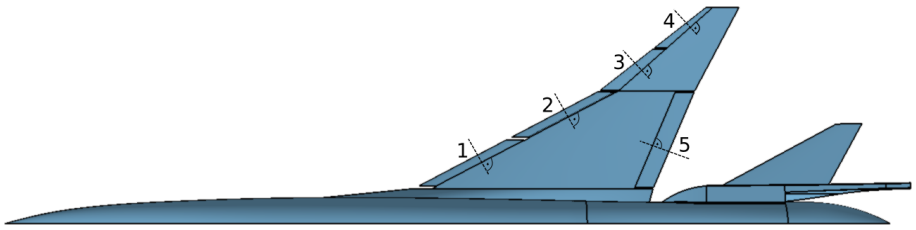

Figure 2: Top view of the configuration used for the optimization with the 5 design variables.

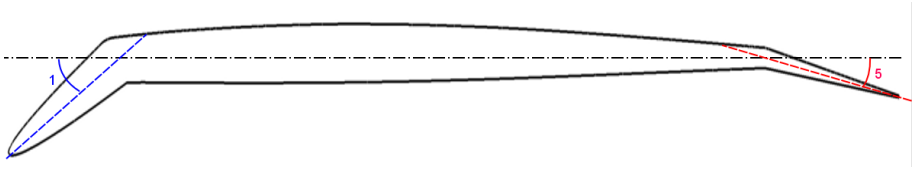

Figure 3: Schematics of the HLD movement. Numbers correspond to the design variables.

The trim constraint is not enforceable as is, since no information exists for the location of the center of gravity (the mass distribution is not frozen yet) and it is therefore not possible to enforce a null pitching moment at the center of gravity. Thus, an alternative formulation is needed in order to retain this constraint. It is chosen to fix the pitching moment to the value found for the clean configuration case (retracted high lift devices) with the horizontal stabilizer in the neutral position (δ=0°), at the design CL; this should be a reasonable assumption and avoid that the optimizer moves towards a solution which is good in terms of L/D but way off trim.

The problem can be simplified with the following assumptions: *a)* the maximum lift over drag ratio always occurs at a lift coefficient smaller then the constraint, and *b)* after its maximum the lift over drag ratio decreases monotonically when increasing CL. With these assumptions the optimization becomes a drag minimization problem at constant lift, with constraints on the pitching moment coefficient Cm and α (table 3).

Variable	Min.	Max.
Leading Edge Flap 1	1°	49°
Leading Edge Flap 2	1°	49°
Leading Edge Flap 3	1°	34°
Leading Edge Flap 4	1°	34°
Trailing Edge Flap	1°	29°

Table 2: Design variables.

Constraint	Type	Value
Cm	=	$Cm_{baseline}$
CL	=	0.5
AoA	<=	12°

Table 3: Constraints of the redefined optimization problem.

3 OPTIMIZATION PROCESS CHAIN

Several building blocks are necessary for the creation of an optimization chain capable of solving an high lift design problem including a trim constraint. The structure of such a chain is outlined in figure 4.

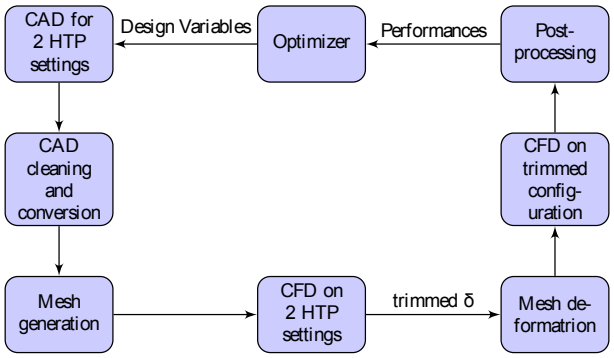

Figure 4: Optimization chain's flowchart.

3.1 CAD modeler

Dassault System's software CATIA is chosen as CAD modeler for shape construction and parametrization. It offers parametric geometry treatment, full scriptability and supports some of the most used geometry description file formats (most notably IGES and STEP). It is the de facto standard in the aeronautical sector despite being available only for the Windows platform and some UNIX flavors (IBM AIX, HP-UX and Solaris).

For the optimization, a simplified geometry without engine nacelles and vertical tails is used.

Once the optimizer sets values for the design variables (the flap settings in this case), those are passed on to CATIA, which modifies the geometry accordingly and saves it in IGES format. Geometry modification and export are performed in batch mode using a Visual Basic script. Additional geometry files are created in this step; they are useful for the creation of the setup files required for the mesh generation.

A CAD converter tool (TranscenData's CADfix) translates the geometry to Flite3D format, which is the format needed by the mesh generator.

3.2 Mesh process

Two unstructured grid generators are intensively used at DLR, namely Centaur and Solar. They were the focus of an extensive study to assess their high lift flow prediction capabilities [6].

The SOLAR mesh generator [7] developed by BAE SYSTEMS, Airbus, and ARA has been chosen since it combines good scripting and automation possibilities, satisfying grid quality, and grid generation speed.

A critical point in the chain is the modification of the mesh settings to take into account the movement of flaps and HTP. Solar uses so called sources that specify the required cell size at each location. The sources for the fixed parts of the geometry (main wing, fuselage) are kept the same during the optimization, while for the movable parts sources are recreated at each step using Solar's auto source manager. This is a tool that automatically creates sources for each

aircraft component. All the auto source manager needs is a so called primitive, a simplified surface that roughly defines the shape of the component to be meshed along with the information on which component (e.g. wing, flap, fuselage, nacelle) it is. To create the primitives, sets of points on the flaps and HTP are exported from CATIA in STEP format. These are then used to build surfaces in a format readable by Solar (icms, a simple ASCII format).

The size of the meshes is about 13.8 million points; the high number of points is justified by the need to resolve the flow in the gaps between the flap sections.

The coupling between the mesh generator and the flow solver consists of some mesh preparations steps. First a tool is used to ensure the conformity of the mesh. After that the mesh quality is improved using a Laplacian smoother; this can noticeably increase the convergence rate of the CFD analysis. Finally the grid is transformed from millimeters (units used in CATIA) to meters (required for the CFD analysis).

3.3 Flow solver

The CFD flow solver DLR-TAU [8] is used for the assessment of the aerodynamic performances. It is a parallel finite volume solver for the Navier-Stokes equations on unstructured grids. In addition to the CFD core package it provides a number of features that can prove useful in an optimization chain like mesh deformation, grid refinement, treatment of chimera grids, just to name a few. Additionally, a python wrapper allows the use of the flow solver and its tools from within a python program, providing an easy way to build complex simulation scenarios.

In the CFD phase the RANS equations are solved using a second order central scheme with artificial scalar dissipation for the space derivatives (with the exception of the convective fluxes of the turbulence equation, for which a second order Roe scheme is used), and a backward Euler scheme for the time derivatives. The equations are closed with the Spalart-Allmaras-Edwards turbulence model. A Cauchy convergence test on drag and pitching moment is used to stop the computation, after which the coefficients are averaged over the last 50 iterations to remove the effect of small oscillations in the results.

All CFD computations are performed using a "target CL" approach, where α is automatically adjusted by the solver during the simulation to match the required CL. The constraint on α is checked at the end of the CFD loop and, if not fulfilled, the configuration is declared unfeasible.

3.4 Trim process

In order to ensure the trimmed state the following strategy is implemented. At the beginning 2 CAD geometries (and 2 meshes) which differ in the HTP setting are created. After carrying out the 2 CFD analyses a linear interpolation of Cm versus the HTP deflection angle δ can be made. This gives a fairly accurate estimation of the required deflection for reaching the trimmed state. At this point a new CFD analysis is required to assess the performances of the trimmed configuration. In order to get this final mesh one can start again from the CAD environment or use a mesh deformation algorithm to rotate the HTP to the required position. The latter has the advantage of being able to retain the mesh topology and restart the CFD analysis from the previous solution, but mesh deformation is only suitable in the case of small displacements, otherwise negative elements could appear in the volume. Mesh deformation is implemented inside TAU and requires a set of points to be moved along with their displacement.

In this work mesh deformation has been used when the required rotation was less than 2° from one of the initial deflections; otherwise a new mesh was created from scratch. In case the required HTP deflection exceeds the maximum allowed value the configuration is declared

unfeasible. It has to be noted that to simplify the problem the HTP is separated from the fuselage. The resulting gap allows the rotation of the HTP without the problems associated with the modification of the intersection line.

All constraints (CL, α, Cm) are treated implicitly in the CFD part of the chain, leaving the optimizer with an unconstrained problem: this requires more time for each evaluation, but the optimization run is expected to converge in less iterations than the constrained problem.

As far as the coupling between the CFD part and the optimizer goes, the only data exchanged between the 2 modules is the value of the objective function (the drag coefficient). To get rid of the small discrepancies in terms of pitching moment value of the trimmed CFD analysis (small in absolute value, but important when comparing the configurations' drag values between each other), a linear interpolation is executed in the CD - Cm space taking into account the final CFD analysis and one of the 2 initial analyses (the closest in terms of δ). The corrected CD value is then passed to the optimizer.

3.5 Optimization framework

An in house optimization framework written in Python, Pyranha [9], is used for the actual optimization run. Various optimization methods are implemented (evolutionary, gradient based, adjoint, gradient free, metamodels, design of experiments) and its modular nature allows for the combination of various method in an optimization run. For example one can start with a scan of the design space, followed by a metamodel approach to find the rough location of the optimum. From there the adjoint method can be used to find the precise location of the optimum.

The "objective evaluation" part of the chain (form CAD to CFD postprocessing) is implemented in Python. This python process is called by the optimizer each time a new configuration has to be assessed.

The implementation is complicated by the fact that the various tools have to run on different computers: CATIA is only available on Windows, Solar only on UNIX, while CADfix and the optimizer can run on both environments. Due to the size of the CFD problem, the mesh generation and the CFD analysis have to be performed on a Linux cluster. It has been decided to run the process on a Linux desktop computer and access remote resources (Windows workstation and Linux cluster) using a python implementation of the SSH protocol (Paramiko) [10].

3.6 Optimization strategies

Two optimization strategies are considered: a Response Surface Method (RSM) that relies on a Regression Kriging approach [11] - which has been recently implemented in Pyranha [13] - and the Simplex method [12]. It is interesting to use both methods since while the RSM method performs a global optimization, the Simplex is inherently local (even though with a large initial simplex size and a smooth objective function the chances of finding the global optimum are good).

Before starting the RSM the design space has to be sampled using a Latin Hypercube Method (LHS); this is required to build a first approximation of the design space. Since all the configurations to be evaluated are defined before the run, the scan can be performed in parallel. Once the first approximate surface created, successive points are added by the RSM method based on 3 criteria:

- Cost function (CF): a new point is added where the response surface predicts the global optimum.

- Kriging Error (KE): a new point is added where the response surface is the most uncertain.
- Expected improvement (EI): a new point is added at the location where the probability of improving the current best element is highest (based on predicted value and its associated uncertainty).

The CF criterion alone would quickly find a local minimum but would miss the global one if not detected by the initial design exploration. The KE method mitigates this problem by refining the model where the uncertainty is highest. The 3rd method tries to combine the best of both worlds, by selecting either points near the current optimum (good predicted value, low uncertainty), or uncertain points (predicted as bad, but with high uncertainty). After the addition of these 3 points, a new response surface is constructed and the process reiterated.

The Simplex method is started using the best configuration found during the Latin Hypercube Sampling, and the size of the initial simplex is chosen as 20% of the variable range in each direction.

4 RESULTS

During the design exploration phase 17 configurations have been assessed, while during the RSM and Simplex optimization 41 and 52 designs have been tested, respectively.

Figure 5 shows the evolution of the design variables for the 3 runs. In the initial phase (LHS), samplings are spread in the entire design space. The RSM method also keeps searching the design space globally focusing on the locations with the highest uncertainties; in particular the boundaries of the design space are searched extensively through the Kriging error criterion and, to a lesser extent, the Expected Improvement criterion. The Simplex method, on the contrary, behaves in a manner typical of a local optimizer: after some initial oscillations it converges to a certain region of the design space.

The different behavior between the optimization methods is also observable in the objective function history (Figure 6). Here the original formulation of the objective function, lift over drag, is used. It has to be recalled however that the optimization is carried out at fixed lift, so this is in essence a drag minimization problem. It is interesting to note that the RSM method finds the second best configuration already in the first cycle (2nd evaluation, CF criterion); this is indicative of the accuracy of the initial (5 dimensional) response surface, which is built with just 17 points. The best solution found by the RSM is obtained at the end of the optimization. The Simplex method keeps improving the solution, and the optimization can be considered converged: the solution could probably be further improved, but the difference in the design variables would be too small compared to the uncertainties in the process.

Method	LE Flap 1	LE Flap 2	LE Flap 3	LE Flap 4	TE Flap	HTP	AoA	L/D
RSM	38.793°	39.107°	33.815°	30.076°	8.113°	-4.97°	10.688°	9.090
Simplex	38.142°	38.599°	33.178°	29.072°	8.110°	-4.92°	10.680°	9.094

Table 4: Best solutions found for each method.

The optimal solutions found by each optimizer are outlined in table 4. Both designs are very similar, with differences less or equal to 1° for each design variable.

A good lift over drag ratio is obtained with a high deflection of the 4 leading edge flap segments, while the trailing edge flap balances the induced pitch up moment. Additionally the

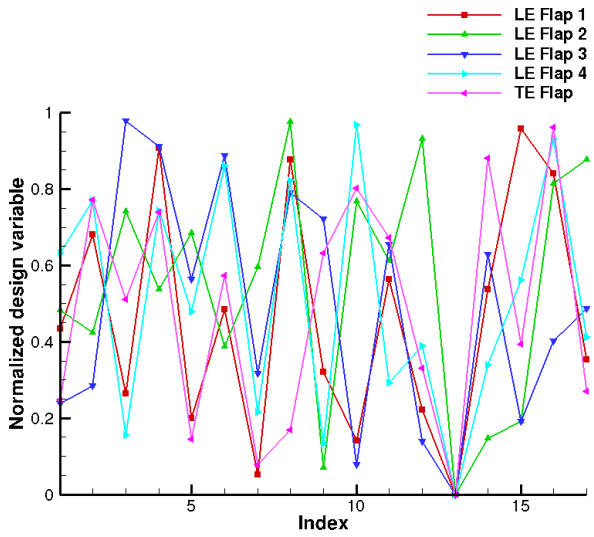

(a) Latin Hypercube Sampling.

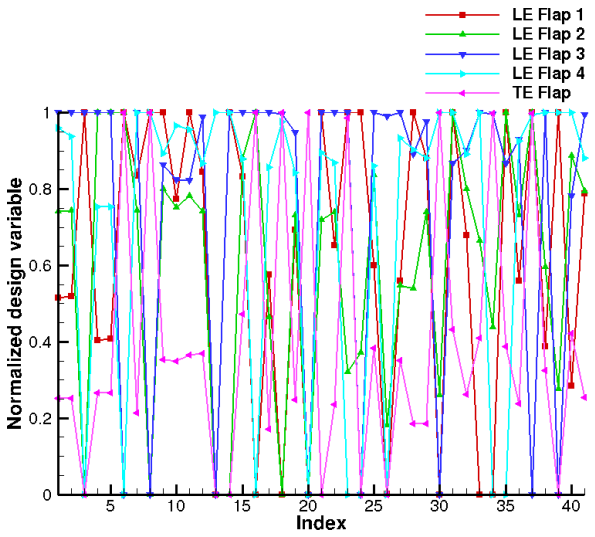

(b) Response Surface Method.

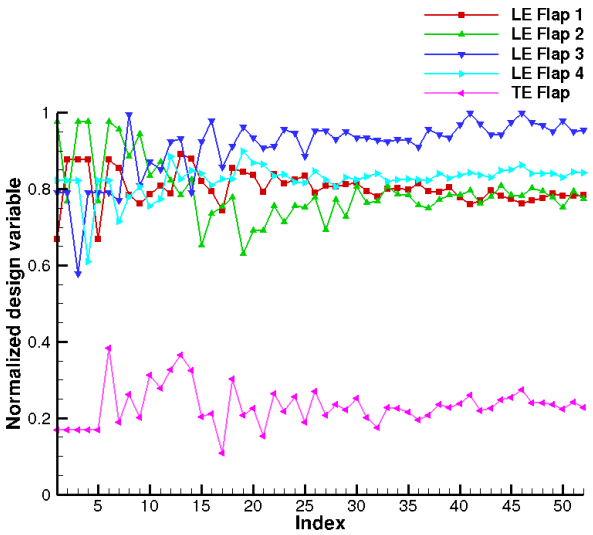

(c) Simplex Method.

Figure 5: Normalized design variable history for the 3 optimization runs.

deflection of the trailing edge flap allows for a reduction of the required angle of attack (the CL versus α curve is shifted up) which is beneficial for the L/D (Figure 7(a)). The (linear) dependency between required α and flap deflection is clearly visible in Figure 7(b). The positive effect of trailing edge flap deflection is balanced by the increased downforce required on the HTP to neutralize the resulting pitch down moment (Figure 7(c)). Both optimizers find an optimal solution with a relatively small trailing edge flap deflection (8°) and a small HTP downforce. From this it emerges that the trim constraint plays a capital role for this optimization problem; without it the optimizers would have found completely different optimal solutions.

Figure 8 shows an analysis of the trim procedure for the configurations analyzed during the LHS run. In the first plot the variation of the pitching moment coefficient as a function of the HTP deflection is depicted, each line corresponding to a configuration (3 CFD computations).

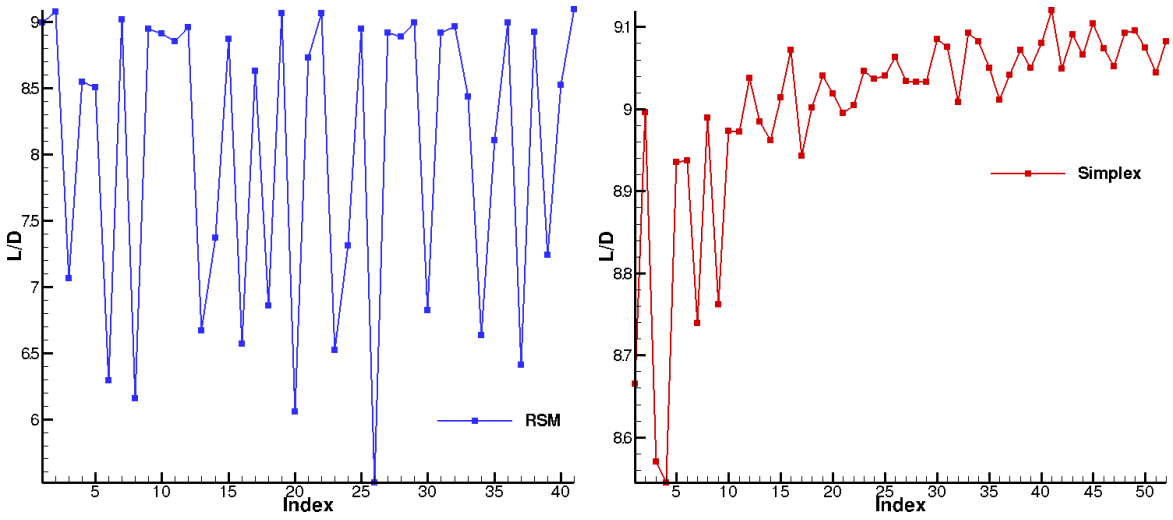

(a) Response Surface Method.

(b) Simplex Method.

Figure 6: Evolution of the objective function for both optimizations.

It is obvious that when considering high deflections ($\delta < 8°$) the linearity of the relation does not hold true anymore since the flow detaches from the HTP. For lower deflection however, the linear assumption taken for the trim condition fulfillment holds true. Moreover, the slope of the curve shows little variation between the configurations even though these are very different from each other in the design exploration phase. This means that after having identified the slope, one of the 2 initial CFD computations could have been avoided, thus reducing the required CPU time. Since the first 2 computations are carried out in parallel, the real time advantage would have been lower.

Trim drag can be divided in three components: the variation of induced drag of the tail, the effect of the wing downwash on the tail, and the variation of induced drag of the wing (see for example [14] for a discussion on trim drag). Neglecting the latter, for evaluating the first two terms it is interesting to look at the lift and drag value of the HTP to see if with an a priori knowledge of the physics some computations could have been avoided.

The induced drag varies with the square of the lift, while the downwash effect is a linear term with respect to lift (at least for small angles). Figure 8(b) shows the HTP drag as a function of the HTP lift (reference values are for the global airplane) for each configuration. Solid lines are quadratic interpolations of the available results while dashed lines are the corresponding extrapolations. The minimum drag is found at a CL value different from zero; the shift to the left is due to the downwash effect. The shift is on average -0.0226 with a standard deviation of 0.0021. The minimum drag value however varies considerably between configurations (average 0.00063, standard deviation 0.00032) so that its use to model the trim drag is not justified. By estimating the quadratic term, however, a single CFD calculation together with the knowledge of the minimum location could provide the necessary information to recreate the HTP lift-drag curve. The mean value of the quadratic term, corresponding to the induced drag contribution, is 0.343, with a standard deviation of 0.0293.

While mathematically correct, the reconstruction of the quadratic curve with just one CFD computation would be inaccurate due to the high standard deviations of the empirical terms ($\sim$10% of the corresponding value). A second CFD would be needed to increase the accuracy,

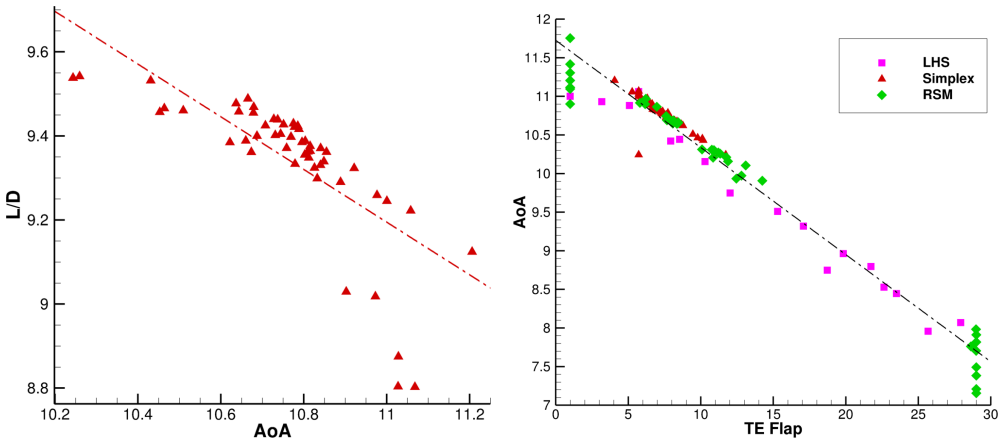

(a) Lift over drag ratio of the wing-body (without HTP) with respect to required angle of attack. Simplex optimization data.

(b) Angle of attack versus trailing edge flap deflection.

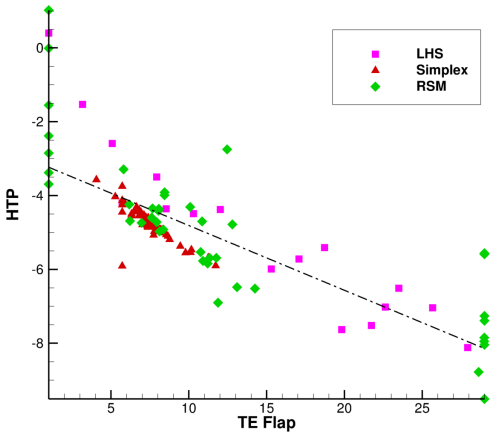

(c) Horizontal tail plane deflection versus trailing edge flap deflection.

Figure 7: Correlations between variables, with linear regressions in dashed lines.

making the model less appealing.

5 OPTIMAL SOLUTION ANALYSIS

The best solution (Simplex result) is analyzed in more details in this section. An analysis of the optimal solution found by the RSM optimizer would be redundant considering the similarity of the results.

In Figure 9 a comparison between the clean configuration and the optimized one in terms of pressure repartition on the suction side of the wing is presented. The optimizer manages to reduce the drag associated with the detached flow caused by the high angle of incidence at the wing leading edge by deflecting the leading edge flaps. The resulting flow is mostly attached on the inboard wing (Figure 10) and notably on the first leading edge flap section whereas small vortices develop on leading edge flap sections 2, 3, and 4. These vortices travel along the flaps

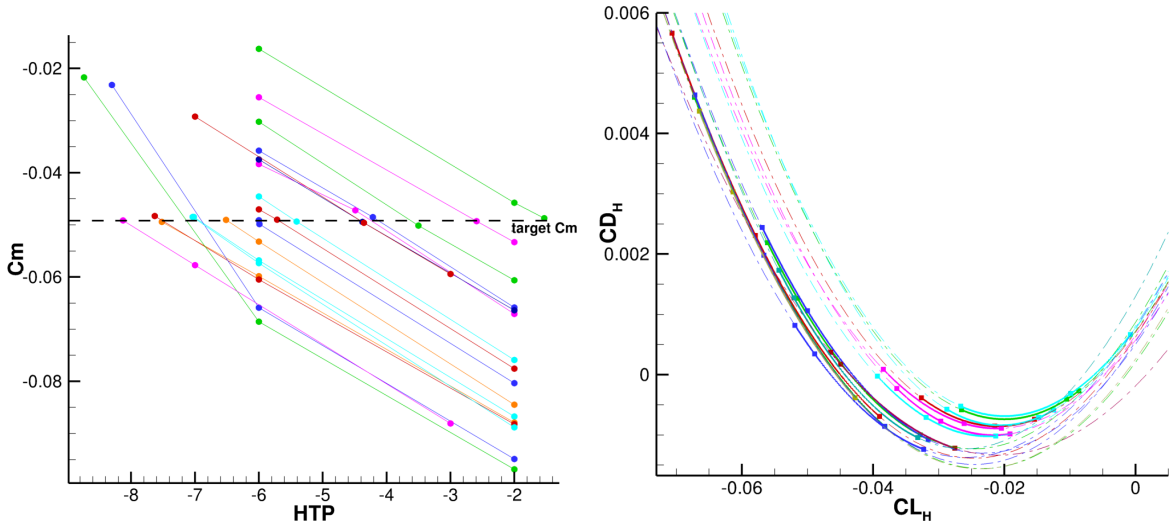

(a) Pitching moment versus horizontal tail plane deflection.

(b) HTP contributions to lift and drag coefficient.

Figure 8: Trim analysis on the configurations tested during the design space exploration phase.

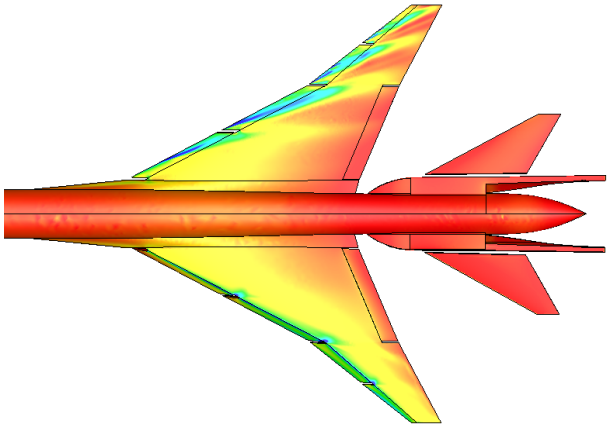

Figure 9: Comparison of the surface pressure coefficient values between the clean configuration (above) and the optimized one (below).

and have a positive effect on the L/D.

A mesh study has been performed to check for the consistency of the CFD results. An analysis of the optimal configuration has been carried out on a refined 30 million points mesh using the same tool chain as for the optimization. The method used in [15] has been applied for the mesh refinement; it allows to keep a constant prismatic layer height. This is a desired propriety when doing mesh studies on hybrid meshes. A computation on the fine grid at the same CL and Cm shows a difference of less than 0.5% for the drag coefficient with respect to the coarser mesh, small enough to consider the optimization results trustworthy.

To make a comparison between the clean configuration and the optimized one, complete polars have been computed. While the clean configuration polar has been computed with a fixed HTP position (δ=0°), the polar for the optimized configuration has been created by adjusting

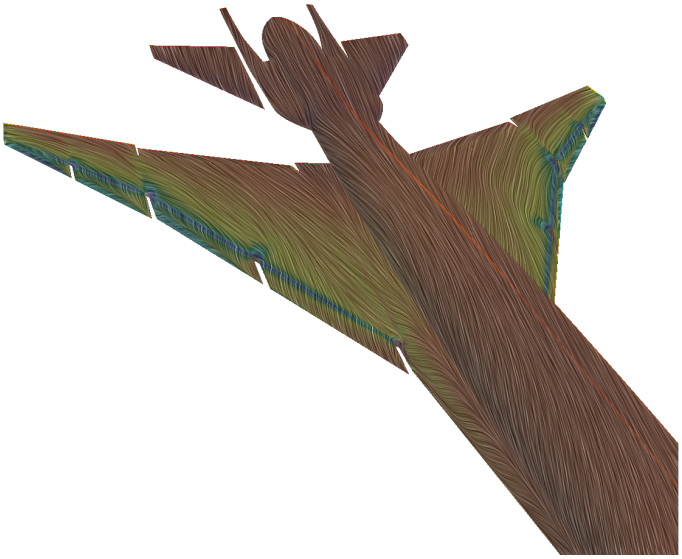

Figure 10: Detail of the surface cf streamlines on the optimized configuration. Surface painted according to the pressure coefficient value.

the Cm to the value found for the clean configuration at the same CL. The resulting polar is shown in Figure 11. The optimized configuration is of course better than the baseline for the design CL, but experiences more drag at low α (lower left corner of the picture). This, although expected, can have an impact on the ground acceleration part of the take-off phase. A more comprehensive measure of the take-off performance could be used in order to include these effects, like for example the balanced field length (BFL). Computationally, this would be more expensive since more aerodynamic data are required. Alternatively, a multipoint optimization [16] could be performed; in this case the weighting between the various objective functions would be critical.

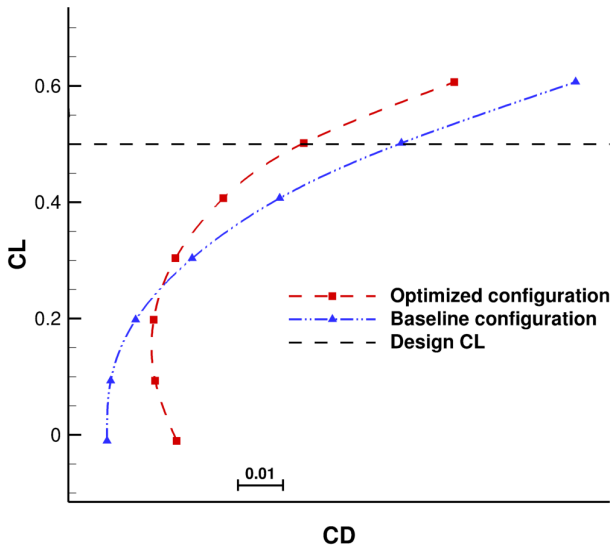

Figure 11: Lift-Drag polar for clean and optimized configuration.

6 CONCLUSIONS

A tool chain for high fidelity aerodynamic optimization has been constructed and outlined in this paper; its ability to directly use and modify CAD geometries coupled with an unstructured mesh approach are the keys to the flexibility of the method. Additionally, the treatment of complex constraints like the trim condition has been demonstrated. As the test case shows, such constraints are of primary importance for drawing meaningful conclusions.

Despite their differences the two optimization processes give similar results for the test case selected and use comparable CPU resources. For a more complex test case (i.e. with more design variables) the RSM method should have a speed advantage over the Simplex.

In the future the optimization chain can be extended to include multidisciplinary optimization (MDO) problems, as well as more complex cases (namely configurations with engine nacelles).

7 ACKNOWLEDGEMENTS

This work has been performed in the frame of a bilateral cooperation between the DLR and JAXA. The authors would like to thank the SST Team of JAXA, and in particular Dr. Dongyoun Kwak, for providing the configuration under study as well as its associated technical data. Acknowledgements also go to Mr. Keisuke Ohira from Ryoyu Systems Co. for the fruitful collaboration on the project. Finally, the authors would like to thank Chunna Li for the support regarding the RSM optimization.

REFERENCES

[1] D. C. Howe: Improved Sonic Boom Minimization with Extendable Nose Spike. AIAA 2005-1014, *43rd AIAA Aerospace Sciences Meeting and Exhibit, ,* Reno, USA (2005).

[2] S. Choi, J. J. Alonso, H. S. Chung: Design of a Low-Boom Supersonic Business Jet Using Evolutionary Algorithms and an Adaptive Unstructured Mesh Method. AIAA 2004-1758, *45th AIAA/ASME/ASCE/AHS/ASC Structures, Structural Dynamics and Materials Conference*, Palm Springs, USA (2004).

[3] S. Z. Pirzadeh: Vortical Flow Prediction Using an Adaptive Unstructured Grid Method. *RTO AVT Symposium on Advanced Flow Management: Part A – Vortex Flows and High Angle of Attack for Military Vehicles*. RTO-MP-069, Loen, Norway (2001).

[4] J.-F. Le Roy, O. Rodriguez: RANS solutions of 70° delta wing in steady flow. *AGARD Report*, RTO-TR-AVT-080, Chapter-16.

[5] U. Herrmann, A. Press, C. Newbold, P. Kaurinkoski, C. Artiles, J. van Muijden, G. Carrier: Validation of European CFD Codes for SCT low-speed high-lift Computations. *19th AIAA Applied Aerodynamics Conference*, Anaheim, USA (2001).

[6] M. Gaffuri, J. Brezillon: Unstructured mesh capabilities for supersonic wing design at low speed conditions. Proceedings of the *ECCOMAS Thematic Conference CFD & OPTIMIZATION*, Antalya, Turkey (2011).

[7] D. G. Martineau, S. Stokes, S. J. Munday, A. P. Jackson and B. J. Gribben: Anisotropic Hybrid Mesh Generation for Industrial RANS Applications, AIAA-paper 2006-534, *AIAA Aerospace Conference*, Reno, USA (2006).

[8] D. Schwamborn, T. Gerhold and R. Heinrich: The DLR TAU-Code: Recent Applications in Research and Industry, *ECCOMAS CFD 2006*, Egmond aan Zee, the Netherlands (2006).

[9] J. Brezillon, A. Ronzheimer, D. Haar, M. Abu-Zurayk, M. Lummer, W. Krüger and F.-J. Natterer: Development and application of multi-disciplinary optimization capabilities based on high-fidelity methods AIAA-2012-1757, *8th AIAA Multidisciplinary Design Optimization Specialist Conference*, Honolulu, USA (2012).

[10] http://www.lag.net/paramiko/

[11] D. R. Jones , M. Schonlau, W. J. Welch: Efficient Global Optimization of Expensive Black-Box Functions. *Journal of Global Optimization*, 13 (1998), 455-492.

[12] J. A. Nelder, R. Mead: A Simplex Method for Function Minimization. *The Computer Journal*, 7 (1965), 308-313.

[13] C. Li, J. Brezillon, S. Görtz: A hybrid approach for surrogate-based aerodynamic optimization with constraints. *ECCOMAS Thematic Conference, EUROGEN 2011*, Capua, Italy (2011).

[14] E. Torenbeek, Synthesis of Subsonic Airplane Design, Delft University Press, 1976.

[15] S. Crippa: Improvement of Unstructured Computational Fluid Dynamics Simulations Through Novel Mesh Generation Methodologies. *Journal of Aircraft*, 48 (2011), 1036-1044.

[16] Č. Ilić, M. Widhalm, J. Brezillon: Efficient polar optimization of transport aircraft in transonic RANS flow using adjoint gradient based approach, *6th European Congress on Computational Methods in Applied Sciences and Engineering*, Wien, Austria (2012).